ISSN 0030-400X, Optics and Spectroscopy, 2016, Vol. 121, No. 6, pp. 810–818. © Pleiades Publishing, Ltd., 2016.
Original Russian Text © A.A. Sobol, V.E. Shukshin, A.I. Zaitsev, 2016, published in Optika i Spektroskopiya, 2016, Vol. 121, No. 6, pp. 871–880.

CONDENSED-MATTER SPECTROSCOPY

Raman Spectroscopy of Crystalline, Glassy, and Molten States of Lead Diborate

A. A. Sobol[a], *, V. E. Shukshin[a], **, and A. I. Zaitsev[b]

[a] *Prokhorov General Physics Institute, Russian Academy of Sciences, Moscow, 119991 Russia*
[b] *Kirensky Institute of Physics, Siberian Branch of Russian Academy of Sciences, Krasnoyarsk, 660036 Russia*
*e-mail: *sobol@lst.gpi.ru, **shukshinve@lst.gpi.ru*

Received March 24, 2016

Abstract—Polarized Raman spectra of single crystals of lead diborate, PbB_4O_7 (PBO), are studied in detail at 300 K. The *TO*-, *LO*-, and *IO*-phonon lines of the A_1, A_2, B_1, and B_2 symmetries in the Raman spectra of this compound are assigned. Changes in the Raman spectra of the internal vibrations of boron–oxygen complexes upon transition from the crystalline to the glassy and the molten states of PBO are observed. On the basis of the obtained results, the regularities in the formation of boron–oxygen complexes in glasses, melts, and crystals of the $PbO \cdot 2B_2O_3$, $SrO \cdot 2B_2O_3$, and $Li_2O \cdot 2B_2O_3$. diborate compositions are analyzed.

DOI: 10.1134/S0030400X16120249

INTRODUCTION

Single crystals of lead diborate, PbB_4O_7 (PBO), were synthesized in [1]. Recently, these crystals have became a subject of interest due to their possible applications in nonlinear optics [2]. Single crystals of strontium diborate, α-SrB_4O_7 (SBO)—a crystal-chemical analog of lead diborate—are of interest due to the combination of unique properties: an unprecedented among oxide materials threshold of the fundamental optical absorption (~130 nm) and high values of nonlinear optical coefficients [3–5].

The structure of SBO and PBO belongs to the orthorhombic crystal structure with space group $Pnm2_1$ and has a number of features. It is based on a three-dimensional lattice formed only of boron–oxygen tetrahedra [6, 7]. The crystal lattice of most borate crystals is formed either of boron–oxygen triangles or bound $[BO_3]$-triangles and $[BO_4]$-tetrahedra [8]. Crystals of PBO and SBO are the only structures containing boron triply coordinated by oxygen [8].

This peculiarity of the structures of the PBO and SBO compounds stimulates interest in their spectroscopic studies to obtain information about the unusual structure of the boron–oxygen fragments in these diborates. In addition, Raman spectroscopy allows one to investigate the influence of the cation (in this case, Sr and Pb) on the structure of boron–oxygen complexes in diborate compounds in the crystalline, glassy, and molten states.

For strontium diborate, a detailed study of the polarized Raman spectra at 300 K and the identification of the symmetry of the vibrational modes in the above-mentioned aggregation states were presented in [9, 10]. The Raman spectra of lead diborate single crystals at 300 K were studied as well [11, 12]. However, these results require clarification, because the data on the vibrational spectra are incomplete due to the use of a limited number of scattering geometries. Also, the results of [11, 12] on the identification of vibrational modes as well as on the appearance of the polarized Raman spectra are contradictory. In this regard, in the present work we carried out a detailed study of the Raman spectra of PbB_4O_7 single crystals at 300 K and identified the symmetry of almost all transverse and longitudinal vibrational modes that was absent in the previous publications. Another aim of this work was to apply Raman spectroscopy to study the structural transformation of boron–oxygen fragments in melting–crystallization processes of diborate compounds, including PbB_4O_7 and SrB_4O_7, which is useful for understanding the existing difficulties in their synthesis from the melt.

MATERIALS AND METHODS

PbB_4O_7 single crystals were grown from the melt with a stoichiometric ratio of components by the Czochralski method. Details of the synthesis process are given in [13]. The sample made for the Raman studies with the use of the X-ray diffraction method had the form of a parallelepiped with the orientation of the edges along the *a*, *b*, and *c* axes. Lead diborate has a rhombic structure $Pnm2_1$ (C_{2v}^7) [7] with two formula

units in the unit cell. This symmetry implies the existence of 72 *TO* vibrations: $19A_1 + 17A_2 + 17B_1 + 19B_2$ corresponding to wave vector $k = 0$ [11], with $A_1 + B_1 + B_2$ being acoustic vibrations. The A_1, B_1, B_2 vibrations are active both in the Raman and IR spectra, while the A_2-symmetry mode is active only in the Raman spectra. In addition to 69 transverse *TO*-vibrations $18A_1 + 17A_2 + 16B_1 + 18B_2$, in Raman spectra one can also record longitudinal *LO*-vibrations of the A_1, B_1, and B_2 symmetries when wave vector **k** of the scattered phonons coincides respectively with the *a, b,* and *c* axes of the crystal. Besides the pure *TO*- and *LO*-phonon lines, Raman spectra should also contain frequencies of the mixed (*IO*) phonons, vector **k** of which makes an angle with the crystallographic axes. This phenomenon is typical for so-called "normal scattering geometries" when the propagation directions of the incident and scattered light are perpendicular. Raman spectra at 300 K were recorded using a SPEX–Ramalog 1403 (Spex-Ramalog 1403) monochromator at a spectral width of the slits of 1 cm^{-1}. The excitation of the Raman signal was carried out by continuous radiation of an argon laser with wavelengths of 488.0 and 514.5 nm and an average power of 0.6 W. Raman spectra recorded for different excitation laser lines showed no impurity luminescence in the studied spectral range.

The Raman spectra at temperatures up to 1400 K were studied with the use of specially developed equipment [14]. The excitation source was a 578.2-nm copper-vapor laser working in the pulsed mode with a frequency of 15 kHz and an average power of 5 W. Raman spectra during the heating and melting were recorded in air; the sample was placed in a platinum crucible inside a vertical tubular furnace heated resistively with a Pt-30%Rh wire. The temperature was measured with an accuracy of 1 K using a Pt-6%Rh–Pt-30%Rh thermocouple attached to the crucible. Raman spectra of the melt were excited and recorded through its upper boundary. For the Raman spectra recorded at high temperatures, the spectral resolution was 3–4 cm^{-1}.

The samples of the $SrO \cdot 2B_2O_3$ and $PbO \cdot 2B_2O_3$ diborate compositions were also prepared by melting the corresponding components. Polycrystalline α-SrB_4O_7 and PbB_4O_7 compounds were synthesized at slow solidification of the melt. To obtain a glass with the same composition the melt was poured on a copper strip. A similar technique was used to prepare a polycrystalline $Li_2O \cdot 2B_2O_3$ sample as a model of a diborate compound with the same ratio of basic and acid oxides as in PbB_4O_7 and SrB_4O_7, but with a different crystal structure and structure of boron–oxygen fragments.

The glass with composition $Li_2O \cdot 2B_2O_3$ was obtained by rapid hardening of the melt between two cooled copper plates.

RAMAN SPECTRA AND IDENTIFICATION OF VIBRATIONS IN PbB_4O_7 SINGLE CRYSTALS AT 300 K

Polarization studies were performed for 12 scattering geometries at both 90° and 180° angles (Table 1). This ensured a reliable identification of the *TO*-vibrations as well as the *LO*- and *IO*-vibrations of the A_1, B_1, and B_2 symmetries that was absent in [11, 12]. Raman spectra of single crystal PbB_4O_7 at 300 K illustrating the vibrational spectra *TO*, *LO*, and *IO* phonons with symmetry A_1, B_1, B_2, and A_2 are shown in Fig. 1. The polarized Raman spectra at 300 K in low (up to 300 cm^{-1}) and high (800–1400 cm^{-1}) frequency ranges are shown in more detail in Fig. 2. The frequencies of the assigned phonons are given in Table 2. The recorded data include $15A_2 + 16B_1 + 17B_2$ lines of *TO*-vibrations, which is close to the result obtained for the vibrational spectrum of PBO on the basis of group theory analysis, $17A_2 + 16B_1 + 18B_2$. At the same time, measurements of polarized Raman spectra for the *TO*-vibrations of the A_1 symmetry resulted in 19 lines instead of the 18 expected from the theory. This contradiction cannot be associated with the registration of the Raman lines, which are forbidden in the scattering geometry for the A_1 vibrations, but may appear in the form of weak traces owing to their large intensity in other scattering geometries. This was carefully checked by analyzing the Raman spectra recorded in different scattering geometries, and the data in Table 2 exclude any wrong assignment of the same frequency to vibrations of different symmetries. It is more likely

Table 1. Scattering geometries used for the identification of the phonons in the rhombic structure of PbB_4O_7 at 300 K. (Directions *X*, *Y*, and *Z* correspond to crystallographic axes [100], [010], and [001], respectively.)

Scattering geometry	Vibration symmetry	Observed component of the scattering tensor
$X(ZZ)\overline{X}$	$A_1(TO)$	α_{zz}
$X(ZZ)Y$	$A_1(TO)$	α_{zz}
$Y(XX)\overline{Y}$	$A_1(TO)$	α_{xx}
$X(YY)\overline{X}$	$A_1(TO)$	α_{yy}
$Z(XX)\overline{Z}$	$A_1(LO)$	α_{xx}
$Z(YY)\overline{Z}$	$A_1(LO)$	α_{yy}
$Z(XY)\overline{Z}$	A_2	α_{xy}
$Y(XY)Z$	A_2	α_{xy}
$Z(XZ)Y$	$B_1(TO)$	α_{xz}
$X(ZX)Y$	$B_1(IO)$	α_{zx}
$Z(YZ)X$	$B_2(TO)$	α_{yz}
$Y(ZY)X$	$B_2(IO)$	α_{zy}

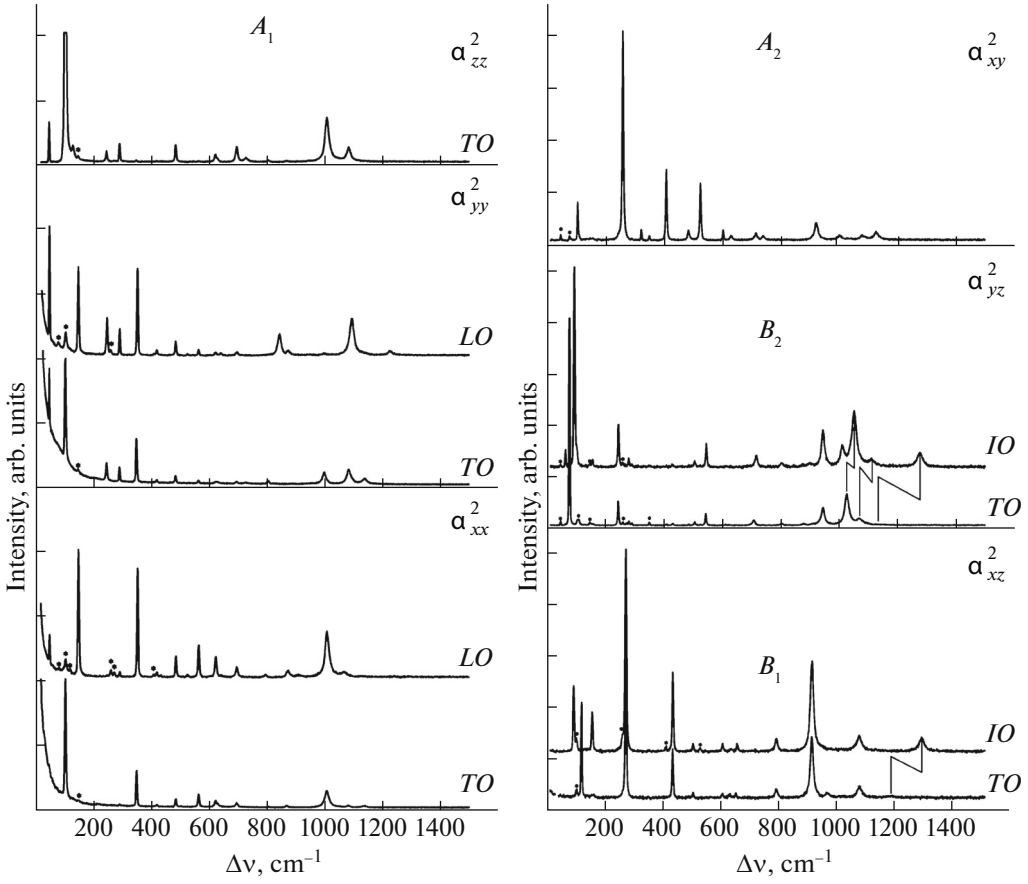

Fig. 1. Polarized Raman spectra of PbB_4O_7 single crystals at 300 K recorded in the scattering geometries in Table 1 to identify the *TO-, LO-,* and *IO*-phonon lines with symmetry A_1, A_2, B_1, and B_2 (the α^2_{ij} components of the scattering tensor from Table 1). The lines that are forbidden in given scattering geometry are labeled with "*".

that the presence of an "extra" A_1 *TO*-line is associated with the effects of anharmonicity or isotopical shift, which were observed earlier in the Raman spectra of borate compounds [15, 16].

Analysis of the spectra of the *LO*- and *IO*-vibrations revealed a number of interesting phenomena. The frequency shift of these vibrations relative to the corresponding *TO*-modes in the range of low and medium frequencies was either absent or did not exceed 10–50 cm^{-1}, whereas in the high frequency range the shift reached a value of 90–130 cm^{-1} (Figs. 1 and 2, Table 2). The same effect was previously observed in the Raman spectra of strontium diborate [10], which is isostructural to PBO.

The Raman spectra of crystalline PbB_4O_7 exhibit an influence of the electro-optic effect on the change of line intensities upon switch from the scattering geometries for the *TO*-phonons to the geometries for the *LO*- and *IO*-phonons. Previously, this phenomenon was observed in the crystals of α-quartz [17], lithium niobate [18], LiB_3O_5 [19], and SrB_4O_7 [10]. A number of lines in the Raman spectra of PBO in the scattering geometries for the *LO* and *IO* phonons exhibit a 10- to 15-fold increase in the intensity as compared with the intensity of the *TO* components of these lines (Fig. 1 and 2).

Owing to this increase in the intensity of the Raman lines of the *LO*- and *IO*-vibrations of a particular symmetry, our attention was attracted to the existence of very weak lines in the Raman spectra for the *TO*-phonons. In the high and low frequency ranges of the Raman spectrum of PBO crystals we identified a number of *TO*-phonon lines, which were not registered in [11, 12]. In addition, a detailed analysis of the Raman spectra in the 12 scattering geometries, corresponding not only to *TO*-phonons, but also to *LO*- and *IO*-phonons, allowed us to exclude the wrong assignment of the same frequency to vibrational modes of different symmetry that is typical for [12].

The present assignment (Table 2) of the symmetry of the vibrational modes in the Raman spectra of PbB_4O_7 is close to the assignment for the SrB_4O_7 single crystals [10], which confirms that these two compounds have an isostructural character. At the same

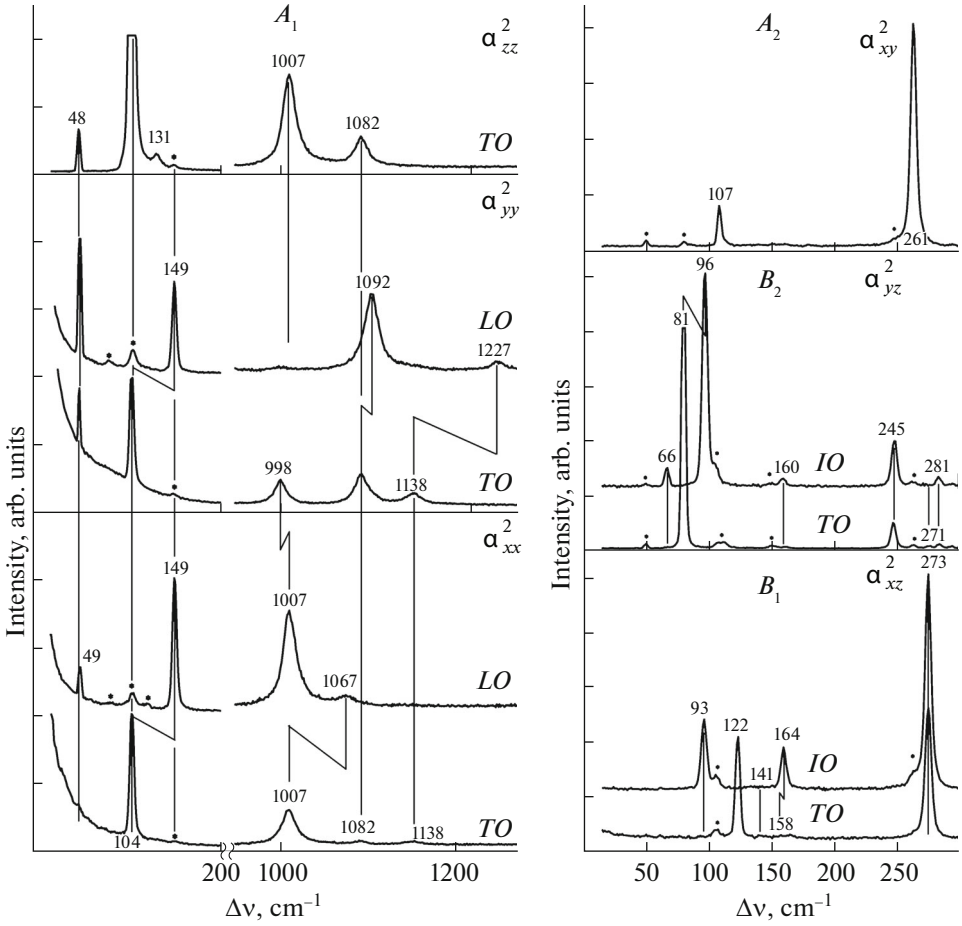

Fig. 2. Low and high frequency ranges of the polarized Raman spectra of PbB_4O_7 single crystals at 300 K from Fig. 1. The lines that are forbidden in given scattering geometry are labeled with "*". The numbers indicate the frequencies of the lines in cm^{-1}. The direct and broken lines indicate the shifts of the *TO-LO* and *TO-IO* phonon lines.

time, the Raman spectra of PBO and SBO differ due to either the different weight or the different character of the partially covalent bonding for Sr and Pb cations. The influence of the cation mass manifests itself in the low frequency range via a significant shift of the threshold of the Raman signal from 104 cm^{-1} in SrB_4O_7 to 48 cm^{-1} in PbB_4O_7, allowing us to assign this signal to external vibrations involving movement of the cations relative to the boron–oxygen anionic motif. In comparison with SrB_4O_7, the high frequency threshold of the Raman spectrum of PbB_4O_7 is only slightly shifted to the low frequency range (not more than 2%) evidencing a weak influence of the cation on the internal vibrations in the boron–oxygen motif.

A difference in the Raman spectra of SrB_4O_7 and PbB_4O_7 is also seen in the redistribution of the relative intensities of the Raman lines in different spectral ranges. This is evident from a comparison of unpolarized Raman spectra of polycrystalline SrB_4O_7 and PbB_4O_7 shown in Figs. 3b and 3c (curve *1*). In the SrB_4O_7 spectrum the most intense lines are in the middle of the frequency range, whereas the PbB_4O_7 spectrum is dominated by the lines in the low frequency range (<200 cm^{-1}). A peculiar influence of cations on the intensity of the Raman spectra for the structures having a sublattice formed of Pb^{2+} ions was observed previously for compounds with a scheelite structure. This phenomenon was explained by the formation of a partially covalent bond between Pb^{2+} and oxygen in the structure of the anionic motif of a number of oxide compounds [20].

RAMAN SPECTRA OF STRONTIUM, LEAD, AND LITHIUM DIBORATES IN THE GLASSY AND MOLTEN STATES

Earlier studies of glasses [15, 21] and melts [22–24] of alkali and alkaline earth borates with different ratio of concentrations of basic and acidic oxides showed that their discrete Raman spectra correspond to the internal vibrations of boron–oxygen fragments with a strong covalent bond. Changes in the structure of these fragments depend on the concentration of the

Table 2. Vibration frequencies (cm^{-1}) corresponding to *LO*- and *IO*-phonons in the Raman spectra of PbB_4O_7 single crystal at 300 K

A_1					A_2	B_1		B_2	
α_{xx}		α_{yy}		α_{zz}	α_{xy}/α_{yx}	α_{xz}/α_{zx}		α_{yz}/α_{zy}	
TO	*LO*	*TO*	*LO*	*TO*	–	*TO*	*IO*	*TO*	*IO*
48	49	48	49	48				66	66
104	149	104	149	104	107	92	93	81	96
–	–	–	–	131		122	–		
–	–	246	248	246	261	141	141	160	160
292	292	291	292	292	324	158	164	245	245
350	353	350	353	350	352	273	273	271	271
420	421	420	420	420	410			281	281
486	486	484	485	486	484	433	433	431	–
564	564	564	564	564	526	501	502	506	507
623	623	623	623	623	604	602	603	544	546
627	641	–	641	627	630	627	631	613	–
696	696	696	696	696	714	649	654		
–	–	–	–	727	740			708	718
806	–	806	844	806		786	786	803	805
868	874	–	874	868		907	909	874	904
–	–	998	1007	–	922	961	–	944	944
1007	1067	–	–	1007	1002	1013	–	–	1010
1082	–	1082	1092	1082	1079	1071	1071	1026	1051
1138	–	1138	1227	–	1125	1179	1284	1070	1110
								1142	1272

α_{ij} labels the components of the scattering tensor that determine the intensity of the Raman lines for the studied scattering geometries.

basic oxide, its type and temperature. The internal vibrations in boron–oxygen complexes were also assigned in the Raman spectra of crystalline borates. Analyzing the Raman spectra, it is convenient to consider the lines of characteristic vibrations of boron–oxygen bonds including terminal (B–O) and bridging (B—O–B) bonds, as well as metaborate and boroxole rings for the fragments consisting of isolated or linked $[BO_3]$-triangles [15–16, 21–24]. The structures containing fragments with linked $[BO_3]$-triangles and $[BO_4]$-tetrahedra also exhibit characteristic vibrations of the rings that consist of these fragments (the six-membered rings) [15, 25]. The presence or absence of lines of such characteristic vibrations in Raman spectra of glasses and melts provided initial grounds for the conclusion of the presence in their composition of the boron–oxygen fragments with a structure similar to the structure of such fragments in crystalline borates [15–16, 22–25]. In this connection, it seemed interesting to analyze the features of the Raman spectra of glasses and melts of strontium and lead diborates, considering the previous detailed studies of the Raman spectra of other diborates, in particular lithium diborate [21–22, 25–27]. Figure 3 (images in the bottom numbered *1, 2,* and *3*) shows the original Raman spectra of polycrystalline, glassy, and melted diborates of lithium, strontium, and lead. For a more detailed demonstration of their features due to the different arrangement of separate boron–oxygen fragments in different aggregate states, the top pair of images (*4* and *5*) show the Raman spectra of the same diborates in the glassy and melted states after the Bose-factor correction.

Let us consider the features of the Raman spectra in Fig. 3a, which were identified earlier in studies of crystalline, glassy, and molten lithium diborates [21, 22, 25, 26].

The high frequency range of the Raman spectra of diborate lithium glass and melt, 1300–1500 cm^{-1}, exhibits a broad polarized band *A* (2–5, Fig. 3a). This band in the Raman spectra of melts and glasses was attributed to the vibration of the terminal B–O bond in the $[BO_3]$-triangles, which form either chains of different length, or a framework. Band *A* indicates the presence of the $[BO_3]$-triangles, one vertex of which has no contact with other boron–oxygen fragments,

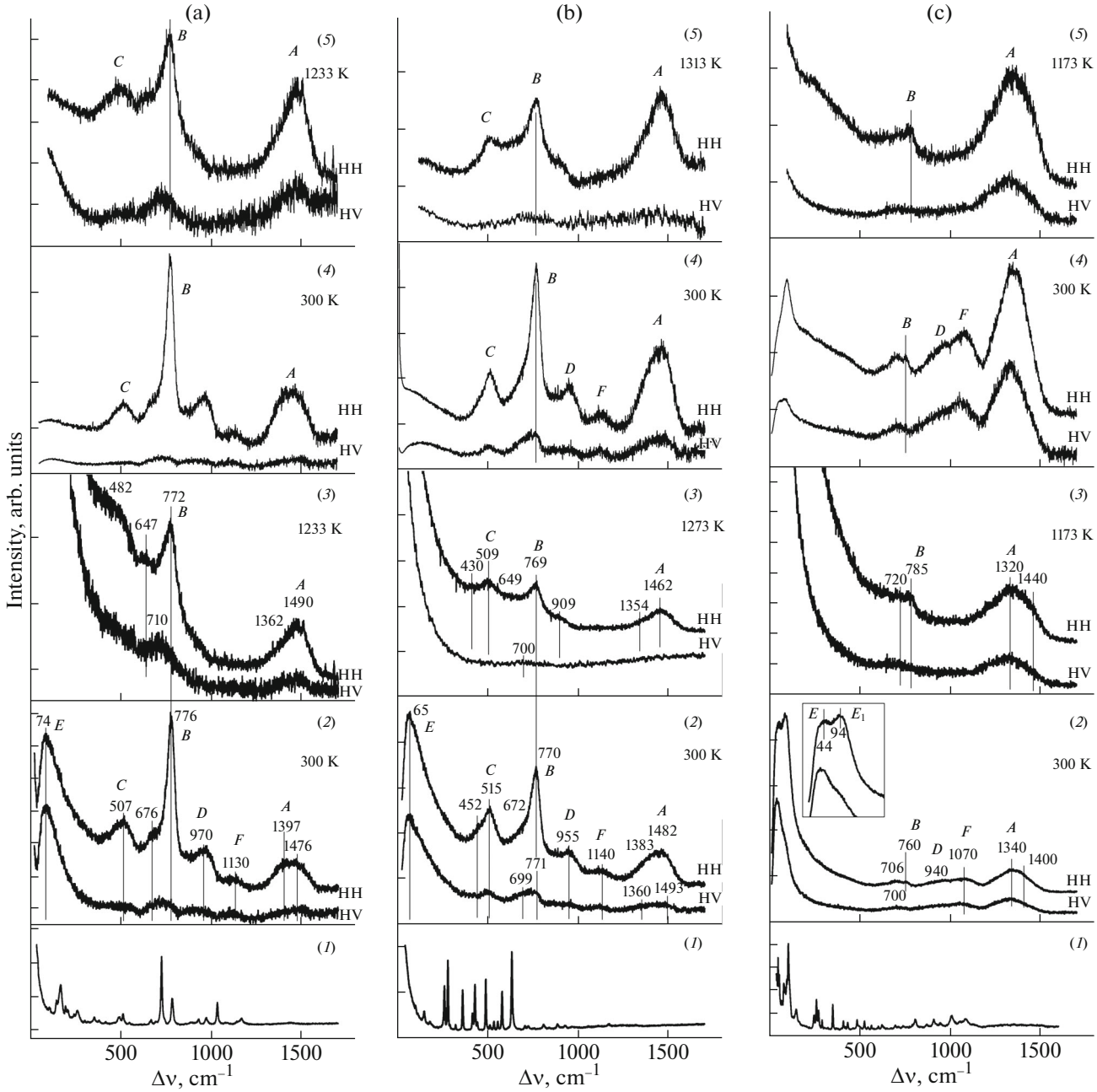

Fig. 3. Raman spectra of (a) lithium diborate, (b) strontium diborate, and (c) lead diborate in polycrystalline (300 K), glassy, and melted states. Original unpolarized Raman spectra of (*1*) polycrystal and original polarized Raman spectra of (*2*) glass, and (*3*) melt; (*4*) spectra of glass (shown in (*2*)) after correction for the Bose factor; and (*5*) spectra of melt (shown in (*3*)) after correction for the Bose factor. The numbers indicate the frequencies of the lines in cm^{-1}. The lines labeled with *A, B, C, D, E,* and E_1 belong to the fragments the nature of which is discussed in the text.

which form a complex anion motif. Because the structure of $Li_2B_4O_7$ crystal contains no $[BO_3]$ triangles with the terminal B–O bond, the high frequency boundary of the $Li_2B_4O_7$ spectrum is considerably lower (below 1200 cm^{-1}) than in the spectra of its glass and melt (*2–5*, Fig. 3a). Thus, the appearance of the *A*-band in the Raman spectra of the lithium diborate glass and melt evidences that part of its anionic motif undergoes restructuring upon melting.

Another feature of the Raman spectra of the melted and glassy lithium diborate is the bands *B* and *C* in the 500–770 cm^{-1} range. Highly polarized and intense band *B* at 770 cm^{-1} deserves attention. This line, according to studies of the Raman spectra of alkaline and alkaline–earth borate glasses [15, 25] and melts [22, 26], is a characteristic vibration of a six-membered ring consisting of linked $[BO_3]$-triangles and

[BO_4]-tetrahedra. As can be seen from Fig. 3a (*2–5*), such fragments should have a rigid structure with a fairly fixed B–O–B angles which exist in the glass and can persist in the melt. The Raman lines in the 500–770 cm^{-1} range of crystalline $Li_2B_4O_7$ spectrum were attributed to the presence of ring-shaped fragments of two linked [BO_3]-triangles and two [BO_4]-tetrahedra. This allows us to consider the *B*- and *C*-lines as indicators of the presence of such ring-shaped [*BC*]-fragments in glassy and molten borates.

In addition to the [*BC*]-fragments, glassy lithium diborate also contains complexes [*DF*], to which the *D* and *F* lines in the 900–1150 cm^{-1} range (*2–5* in Fig. 3a) are attributed [15, 21, 25]. The *D* and *F* lines completely disappear from the Raman spectra upon the transition from the glassy state of lithium diborate at 300 K to its molten state (*2–5* in Fig. 3a). At the same time, in the spectra of the melt recorded at the lithium diborate melting temperature, the lines of the ring-shaped [*BC*]-fragments are preserved, but their intensity is redistributed with band A showing stronger growth upon melt overheating by 150–200 K [22, 26].

Such temperature behavior of the lines of the [*BC*]- and [*DF*]-fragments confirms that, along with [BO_3]-triangles, their composition includes [BO_4]-tetrahedra, which transform into the boron–oxygen triangles at high temperatures. In addition to the Raman spectroscopy method, the thermal instability of the tetrahedral groups in various borates and their transformation into [BO_3]-fragments have also been proven by other experimental methods [28, 29]. If the *B* band is widely recognized as a characteristic vibration of the six-membered ring, the question of the structure of the fragments corresponding to the *D* and *F* bands in the Raman spectra is controversial. Given the disappearance of these bands from the Raman spectra of melted borates at relatively low temperatures, it can be considered that the [*DF*]-complexes includes mixed fragments of [BO_4]- and [BO_3]-groups with an arrangement differing from that for the ring-shaped [*BC*]-fragments.

The low frequency range of the Raman spectrum (65–75 cm^{-1}) of glassy lithium diborate exhibits an intense broad band *E* (*2* in Fig. 3a), which is a distinctive feature of the Raman spectra of the glassy state (the Boson peak [30]).

As can be seen comparing Figs. 3a and 3b (*2–5*), the Raman spectra of glassy and molten diborates of lithium and strontium are completely similar in the number of observed bands, their frequencies, the ratio of their intensities and polarization, as well as in character of the temperature-induced change of the Raman spectra upon the transition from the glassy to the molten state. This allows us to conclude that the anionic motif in the $SrO \cdot 2B_2O_3$ и $Li_2O \cdot 2B_2O_3$ glasses and melts contains the same set of boron–oxygen fragments with a specific structure and the ratio of their concentrations.

The crystal structure of α-SrB_4O_7 does not include the [BO_3]-triangles, as well as mixed fragments of the [BO_3]-triangles and [BO_4]-tetrahedra, whereas the lines of these groups are seen in the Raman spectra of strontium diborate glass and melt (Fig. 3b). This fact indicates that melting of the α-SrB_4O_7 crystal completely transforms this peculiar construction of the anionic motif consisting solely of [BO_4]-tetrahedra.

At first glance, the formation of a boron–oxygen motif in lead diborate glass and melt would have to be the same as in the cases of lithium and strontium diborates. However, the Raman spectra of $PbO{\cdot}2B_2O_3$ composition in the glassy and melted states (*2–5* in Fig. 3c) differ significantly from the spectra of lithium and strontium diborates in the glassy and melted states (*2–5* in Figs. 3a and 3b). In addition to boson peak *E*, the low frequency range of the spectrum of the $PbO \cdot 2B_2O_3$ glass, exhibits strongly polarized band E_1 (*2* in Fig. 3c). In the Raman spectra of lead diborate glass and melt, it is also possible to assign features of the same characteristic vibrations of boron–oxygen fragments as in the spectra of $SrO \cdot 2B_2O_3$ and $Li_2O \cdot 2B_2O_3$, namely, the *A*-, *B*-, *D*-, and *F*-bands, considering such characteristics as frequency, polarization, and change in intensity with temperature. At the same time, if the narrow and strongly polarized *B*-band dominates in the spectra of lithium and strontium diborates in the glassy and melted states, the intensity of this line in the spectra of lead diborate in these aggregation states is very small (spectra *2–5* in Figs. 3b and 3c). On the contrary, the *A*-band, which is less intense in the Raman spectra of lithium and strontium diborates in the glassy and melted states, dominates in the spectra of $PbO \cdot 2B_2O_3$. In addition, the *D*- and *F*-bands in the spectrum of the $PbO \cdot 2B_2O_3$ glass also have a relatively large intensity in comparison with $SrO \cdot 2B_2O_3$ and $Li_2O \cdot 2B_2O_3$ glasses (spectra *2* in Figs. 3c, 3a, and 3b).

Thus, in the first approximation, the analysis of the Raman spectra of $Li_2O \cdot 2B_2O_3$, $SrO \cdot 2B_2O_3$, and $PbO \cdot 2B_2O_3$ compositions in the glassy and melted states reveals the same set of boron–oxygen fragments. At the same time, the ratios of the relative amounts of these fragments in the case of Pb^{2+} significantly differ from those for Li^+ and Sr^{2+}. In particular, glassy and molten lead diborate contain a very small amount of the ring-shaped [*BC*]-fragments and a large amount of the [BO_3]-triangles, with one vertex forming no bridging B–O–B bonds (the *A*-fragments). The reason for this may be a relatively high value of the partially covalent bond between Pb and oxygen in the composition of the boron–oxygen fragments, which shifts the equilibrium in the melt toward the preferential formation of complexes containing triple-coordinated boron. A large degree of the covalent character in the Pb–O

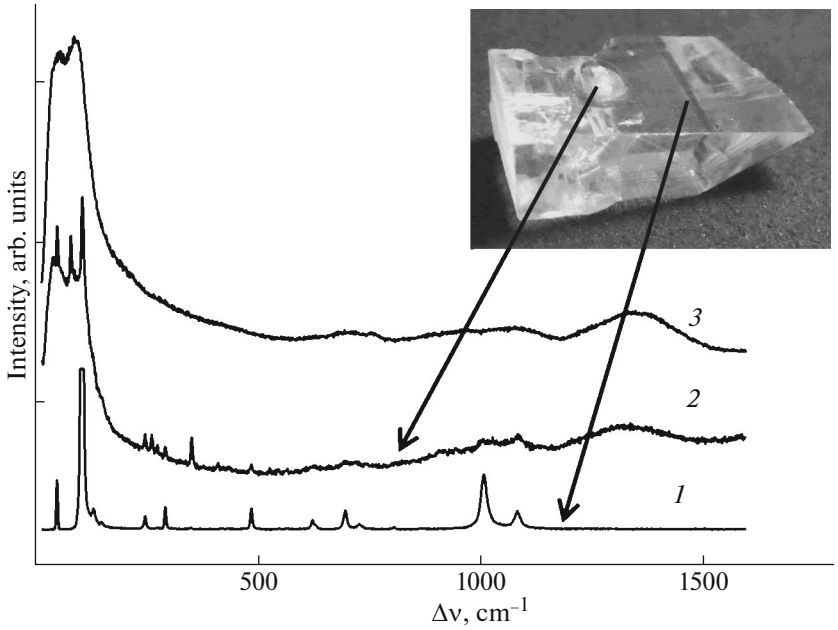

Fig. 4. Raman spectra of (*1*) surface of a PbB_4O_7 single-crystal, (*2*) drop of the melt on its surface, and (*3*) glassy lead diborate. Spectra were recorded at 300 K. Arrows indicate the places on the sample (inset) where the Raman spectra were recorded.

bond is a probable explanation for the appearance of low frequency band E_1 in the Raman spectrum of lead diborate glass (*2* in Fig. 3c). In this case, bonding of Pb with "nonbridging" oxygen in the B–O groups would result in the formation of a partially ordered structure with the Pb–O vibrations being localized within a narrow interval of the low-frequency range.

The structure of PbB_4O_7 is a crystallo-chemical analog of α-SrB_4O_7 and contains only fragments of vertex-linked $[BO_4]$-tetrahedra; as follows from the analysis of Raman spectra, in melted PbB_4O_7 these fragments are completely transformed into fragments consisting of linked $[BO_3]$-triangles. Accordingly, crystallization of the melt is to be accompanied by the inverse structural transformation of the anionic motif. Given the strong difference in the structure of the individual fragments of melted and crystalline PBO, such a transformation is hampered in both homogeneous and heterogeneous processes of nucleation. This explains the high propensity of the $PbO \cdot 2B_2O_3$ melt to glass transition even at relatively slow cooling and in the presence of a contact with the surface of PbB_4O_7 crystal. This phenomenon is illustrated in Fig. 4.

This figure shows a photograph of a PbB_4O_7 single crystal with a transparent droplet of $PbO \cdot 2B_2O_3$ on the crystal surface which was solidified after separation of the crystal from the melt. Figure 4 also shows Raman spectra of the droplet and crystal surfaces at 300 K. As follows from the analysis of these spectra, the solidified droplet is a partially crystallized glass consisting of randomly oriented PbB_4O_7 nanocrystals. It is for this reason that the Raman spectrum of such crystallites in the glassy droplet noticeably differs from the spectrum of a oriented face of the single crystal. Thus, the single crystalline surface, which is in contact with the droplet, does not act as a seed for the growth of the crystallites with the same orientation as the face of the single crystal.

CONCLUSIONS

Analysis of polarized Raman spectra recorded at different scattering geometries of the PbB_4O_7 single crystal resulted in identification of $15A_2 + 16B_1 + 17B_2$ lines that is close to the theoretical spectrum of *TO*-vibrations for the $Pnm2_1$ structure ($17A_2 + 16B_1 + 18B_2$). At the same time, for the A_1 symmetry, the number of recorded lines is 19 instead of 18 that is predicted by the theory.

Replacement of Sr for Pb in the $Pnm2_1$ structure significantly shifts the spectrum of external lattice vibrations to the low frequency range, while the spectrum of internal vibrations in the boron–oxygen motif virtually remains the same.

Similarly to the Raman spectra of α-SrB_4O_7, the spectra of PbB_4O_7 show a significant shift in the frequencies of the *LO*- and *IO*-vibrations (up to 130 cm^{-1}) and the increase in the intensity of these lines as compared to the Raman spectra of the *TO*-phonons.

The study of Raman spectra showed that the peculiar arrangement of boron–oxygen complexes in the structure of SrB_4O_7 and PbB_4O_7 crystals completely transforms upon their melting. At the same time, for

lead diborate in the molten and glassy states, the process of formation of new complexes significantly differs from the same process in the case of strontium and lithium diborates.

ACKNOWLEDGMENTS

This work was performed with financial support from RFBR, research project no. 13-02-00707.

REFERENCES

1. J. F. H. Nicholls, B. H. T. Chai, D. Russell, and B. Henderson, Opt. Mater. **8**, 185 (1997).
2. A. A. Kaminskii, L. Bohaty, P. Becker, J. Liebertz, L. Bayarjargal, J. Hanuza, H. J. Eichler, H. Rhee, and J. Dong, Laser Phys. Lett. **4**, 660 (2007).
3. S. Block, A. Perloff, and C. E. Weir, Acta Crystallogr. **17**, 314 (1964).
4. K. Machida, H. Hata, K. Okuno, G. Adachi, and J. Shiokawa, J. Inorg. Nucl. Chem. **41**, 1425 (1979).
5. H. Huppertz, Z. Naturforsch. B **58**, 257 (2003).
6. P. Trabs, F. Noack, A. S. Aleksandrovsky, A. I. Zaitsev, and V. Petrov, Opt. Lett. **41**, 618 (2016).
7. D. L. Corker and A. M. Glazer, Acta Crystallogr. B **52**, 260 (1996).
8. N. I. Leonyuk and L. I. Leonyuk, *Crystal Chemistry of Anhydrous Borate* (Mosk. Gos. Univ., Moscow, 1983) [in Russian].
9. V. I. Zinenko, M. S. Pavlovskii, A. I. Zaitsev, A. S. Krylov, and A. S. Shinkarenko, J. Exp. Theor. Phys. **115**, 455 (2012).
10. A. A. Sobol', V. E. Shukshin, and A. I. Zaitsev, Opt. Spectrosc. **121**, 25 (2016).
11. Y. Wang, M. Feng, H. Wang, P. Fu, J. Wang, X. Cao, and G. Lan, J. Phys.: Condens. Matter **19**, 436207 (2007).
12. A. A. Kaminskii, L. Bohaty, P. Becker, J. Liebertz, L. Bayarjargal, J. Hanuza, H. J. Eichler, H. Rhee, and J. Dong, J. Raman Spectrosc. **39**, 409 (2008).
13. A. I. Zaitsev, A. S. Aleksandrovsky, A. S. Kozhukhov, L. D. Pokrovsky, and V. V. Atuchin, Opt. Mater. **37**, 298 (2014).
14. Yu. K. Voron'ko, A. B. Kudryavtsev, V. V. Osiko, and A. A. Sobol', in *Growth of Crystals,* Ed. by Kh. S. Bagdasarov and E. B. Lube (Consultant Bureau, New York, 1991), Vol. 16, p. 199.
15. T. W. Bril, Philips Research Rep., No. 2 (1976).
16. Yu. K. Voronko, A. V. Gorbachov, V. V. Osiko, A. A. Sobol, R. S. Feigelson, and R. K. Route, J. Phys. Chem. Solids **54**, 1579 (1993).
17. J. D. Masso, C. A. She, and D. F. Edwards, Phys. Rev. B **1**, 4179 (1970).
18. A. S. Barker, Jr. and R. Loudon, Phys. Rev. **158**, 433 (1967).
19. Yu. K. Voron'ko, A. A. Sobol', and V. E. Shukshin, Opt. Spectrosc. **115**, 863 (2013).
20. T. T. Basiev, P. G. Zverev, A. Ya. Karasik, V. V. Osiko, A. A. Sobol', and D. S. Chunaev, J. Exp. Theor. Phys. **99**, 934 (2004).
21. E. I. Kamitsos, M. A. Karakassides, and G. D. Chryssikos, Phys. Chem. Glasses **28**, 203 (1987).
22. Yu. K. Voron'ko, A. V. Gorbachev, A. B. Kudryavtsev, and A. A. Sobol', Inorg. Mater. **28**, 1368 (1992).
23. Yu. K. Voron'ko, A. V. Gorbachev, A. B. Kudryavtsev, and A. A. Sobol', Inorg. Mater. **28**, 1361 (1992).
24. Yu. K. Voron'ko, A. A. Sobol', and V. E. Shukshin, J. Mol. Struct. **1008**, 69 (2012).
25. W. L. Konijnendijk, Philips Research Rep. No. 1 (1975).
26. Yu. K. Voron'ko, A. A. Sobol', and V. E. Shukshin, Inorg. Mater. **49**, 923 (2013).
27. A. A. Sobol', V. E. Shukshin, and L. V. Moiseeva, Opt. Spectrosc. **121**, 32 (2016).
28. S. Sen, J. Non-Cryst. Solids **253**, 84 (1999).
29. O. Majerus, L. Cormier, G. Calas, and B. Beuneu, Phys. Rev. B **67**, 024210 (2003).
30. V. K. Malinovski and A. P. Socolov, Solid State Commun. **57**, 757 (1986).

Translated by V. Alekseev